Dalton Transactions

Accepted Manuscript

This article can be cited before page numbers have been issued, to do this please use: K. Choy and D. Choi, *Dalton Trans.*, 2017, DOI: 10.1039/C7DT01120B.

ROYAL SOCIETY OF CHEMISTRY

rsc.li/dalton

View Article Online
DOI: 10.1039/C7DT01120B

Electrochemical Effect of Various Si/Zr Molar Ratios for Anode Materials in Lithium-ion Batteries

Dong-Woong CHOI[(1)(2)], Kwang-Leong CHOY[(1)]*

(1) UCL Institute for Materials Discovery, (2) Department of Chemistry
University College London, WC1E, 7JE, United Kingdom
*Corresponding Author: k.choy@ucl.ac.uk

Abstract

The aim of this study was to unveil the mechanisms through electrochemical analysis and to understand the effect of various Si/Zr molar ratios (Si/Zr=0.5, 1, and 2) on the performance of SiO_2/ZrO_2 (SSZ) anode materials with these mechanisms. The 2-SSZ (Si/Zr=2) electrode had a much higher capacity than that of the 0.5- or 1-SSZ (Si/Zr=0.5 or 1) electrode. It exhibited superior cycling performance when compared to commercial graphite (theoretical capacity of 372 mAh g^{-1}). The 2-SSZ had a capacity of 461 mAh g^{-1} at a high current density of 100 mA g^{-1} over 30 cycles. These characteristics are due to the effects from each of the different reversible materials formed by the SSZs. Zr_2Si and Zr_5Si_3, ZrSi, or $ZrSi_2$ were formed by the 0.5-, 1-, and 2-SSZ, respectively, which would affect the reversible storage capacity. $ZrSi_2$ provided an increase in the possible reaction area for the guest species (lithium ions) at the empty interstitial site in the host materials as well as a large space for accommodating a volume change. It was supportive by maintaining the lattice constant and reducing the ratio of the structure distortion. Furthermore, the 2-SSZ structure consisted of an overall amorphous structure with a crystalline structure related to the Zr-O-Si bond unlike the 0.5- and 1-SSZ which had an overall crystalline structure. Such combined structure of 2-SSZ was advantageous in providing a good capacity due to the amorphous structure and an efficient pathway for electron transport and little pulverization due to the crystalline structure. This structure led to its superior performance and long-life span.

Keywords

Si/Zr, Lithium ion battery, batteries, SiO_2, ZrO_2

View Article Online
DOI: 10.1039/C7DT01120B

1. Introduction

Rechargeable lithium ion batteries (LIBs) with efficient outperformance are the most extensively used of various battery types, including nickel or lead-acid batteries [1, 2]. When compared to these batteries, LIBs are characterized by high energy density and power density, low self-discharge, low maintenance, lightweight, and long lifespan. The range of applications for LIBs is rapidly widening into areas such as flexible electronics and electric vehicles (EVs) [3-5]. Therefore, LIBs have been extensively employed since the first commercial products in 1991, and it is believed that this demand will continue to increase. According to Nexeon, one of the LIB companies in the UK, the LIB market is predicted to grow to 60 billion dollars by 2020 [6].

Currently, many portable electronic devices with many embedded convenient and elaborate functions, have been produced. The trend in recent lithium ion battery (LIB) research regarding energy sources has also been progressing toward development of more efficient and powerful electronic systems [1, 2]. This ever growing demand triggers expensive research for energy sources with power densities much higher than for conventional lithium ion batteries.

Graphite has been widely used as the typical anode material in conventional LIBs due to its advantages of low cost and high chemical stability. However, its theoretical capacity is 372 mAh g^{-1}, which is quite low given the increasing demands of a rapid shifting technology. To reduce this gap, novel materials exhibiting higher capacity are required to address the need for higher energy density and longer cycle life. Thus, various materials with high capacity (e.g. metals, metal alloys, and metal oxides) have been researched for use as anode materials [7, 8].

Materials made of silicon (Si) have attracted much attention in LIB research. The combination of Si with lithium (Li) ions helps LIBs have a much higher specific capacity (4,200 mAh g^{-1}), which brings us one step closer to a highly upgraded commercial LIB. However, the Si material shows a large volume change during repeated intercalation and deintercalation of lithium ions, which causes the anode to crack and pulverize. This eventually leads to a poor life cycle, low mechanical stability, and a drastic drop in LIB performance. Structural modifications such as sandwich-structured Si [9], Si-nanotubes (SiNTs) [10], hierarchical nanoporous Si [11], and Si-nanowires (SiNWs) [12, 13] have been introduced to manage such issue. However, preparation of such products requires many

View Article Online
DOI: 10.1039/C7DT01120B

complex steps. Because of that, it is laborious to prepare Si materials of such peculiar design . These result in costly products.

In order to resolve these issues, metallic oxide-based materials have been proposed, such as SiO_2 and ZrO_2. Recent studies suggest that SiO_2 reacts with lithium ions and that it has a high storage capacity and cyclability. For instance, a carbon coated SiO_2 composite delivers an initial discharge capacity of 536 mAh g^{-1} and a capacity of about 500 mAh g^{-1} at the 50th cycle [14]. Commercial SiO_2 reacts with lithium ion between 0.0 and 1.0 (vs Li/Li^+) and shows a capacity of 400 mAh g^{-1} [15]. The benefits of these composites have been attributed to the formation of Li_2O or Li_4SiO_4 in the first discharge cycle, which then suppressed large volume change of host materials. Furthermore, the cost of SiO_2 is less than that of Si or SiO because it is much more abundant. Therefore, SiO_2 is attractive as a new candidate material for negative electrodes. In the case of positive electrodes, the mixing of SiO_2 and $LiCoO_2$ form Li_2CoSiO_4, which provided high capacity retention, with 130 mAh/g in the range 2.7-4.3 V, at 0.1 mA cm^{-2} [16]. ZrO_2 was found to suppress solid electrolyte interface (SEI) formation and enhanced electron transport at the negative electrode. The use of ZrO_2 on $Li_4Ti_5O_{12}$ could improve the specific capacity, cyclability, and rate capability of $Li_4Ti_5O_{12}$, and this composite delivered the best initial discharge capacity of about 350 mAh g^{-1} between 0.1 and 2.5 V, at the current density of 200 mA g^{-1} [17]. For the positive electrode, when ZrO_2 coated on $LiCoO_2$ is compared with uncoated $LiCoO_2$; $ZrO_2/LiCoO_2$ would provide enhanced capacity retention in a high voltage range [18, 19]. Moreover, coated ZrO_2 showed a protective effect on the surface of the pristine LiCoO2 electrode [20].

In this paper, we prepared three SSZs with different molar ratios of Si/Zr=0.5, 1, and 2, and investigated the effect of Si/Zr based on those performance. Then these were analyzed using the approach of thermodynamic and electrochemical studies. To the best of our knowledge, no studies have been reported for the effect of Si/Zr on SSZ in the lithium ion batteries, and if so, this would be the first report regarding the experimental investigationEach SSZ was denoted as 0.5-, 1-, and 2-SSZ. The electrochemical performances of SSZ, including galvanostatic charge/discharge, was extensively evaluated in half cells.

2. Experimental

2.1. Preparation of composite materials

View Article Online
DOI: 10.1039/C7DT01120B

SiO_2/ZrO_2 with different mole ratios of Si/Zr (=0.5, 1, and 2) were synthesized using $ZrOCl_2 \bullet 8H_2O$, $(NH_4)_2CO_3$, and Na_2SiO_3 according to reference [21]. $ZrOCl_2 \bullet 8H_2O$ was dissolved in DI water, and $(NH_4)_2CO_3$ was dripped in the solution until zirconyl carbonate was formed. The precipitate was then washed to remove chloride ions. The $(NH_4)_2CO_3$ was added and stirred until reaching pH 8, and then Na_2SiO_3 was introduced into the precursor solution. After the gel was formed, it was kept overnight and aged at 80°C and 100 ^{o}C for several days. In order to remove the surfactant, the precipitate was washed with DI water several times. Then the product was filtered. The mixture was heated at 90 ^{o}C to dry DI water and 1050 ^{o}C to make different structures in SSZ samples. Here, 0.5-SSZ, 1-SSZ, and 2-SSZ represent the synthesized SiO_2/ZrO_2 with mole ratio of Si/Zr=0.5, 1, and 2, respectively.

2.2. Characterization

The structure of the prepared samples was analyzed using X-ray diffraction (STOE, STADI-P) with Mo-Kα1 radiation. The synthesized materials were measured by Fourier Transform Infrared spectroscopy (FT-IR, Spectra Two of Perkin Balmer). The recorded wave number range of the FT-IR spectra was from 400 to 4000 cm^{-1}. The microstructure and morphology were observed using high-resolution transmission electron microscopy (HRTEM, JEM-2100F and JEM-2100 Plus) and field-emission scanning electron microscopy (FESEM, JSM-6700F).

2.3. Electrochemical measurement

The negative electrode was composed of the active materials (SSZ), carbon black (Super P), and binder (polyvinylidene fluoride, PVDF), with a weight ratio of 50:30:20. These were then mixed in N-methylpyrrolidone (NMP) and spread on a Cu-foil using a Dr. Blade casting. The loading density on Cu-foil was around 2 mg cm^{-2}. This film was dried in a vacuum oven. Li-foil was applied as the counter electrode. The electrolyte solution was 1M $LiPF_6$ in ethylene carbonate (EC): dimethylcarbonate (DMC) with a volume ratio of 1:1, and Whatman was used as a separator. CR 2032 type cells were assembled with these components in an Argon-filled glove box. Galvanostatic charge/discharge measurement was performeded using an Arbin battery tester within the potential range of 0.001-2.0 V (vs. Li/Li^+) at a current density of 100 mA g^{-1}.

View Article Online
DOI: 10.1039/C7DT01120B

3. Results and discussion

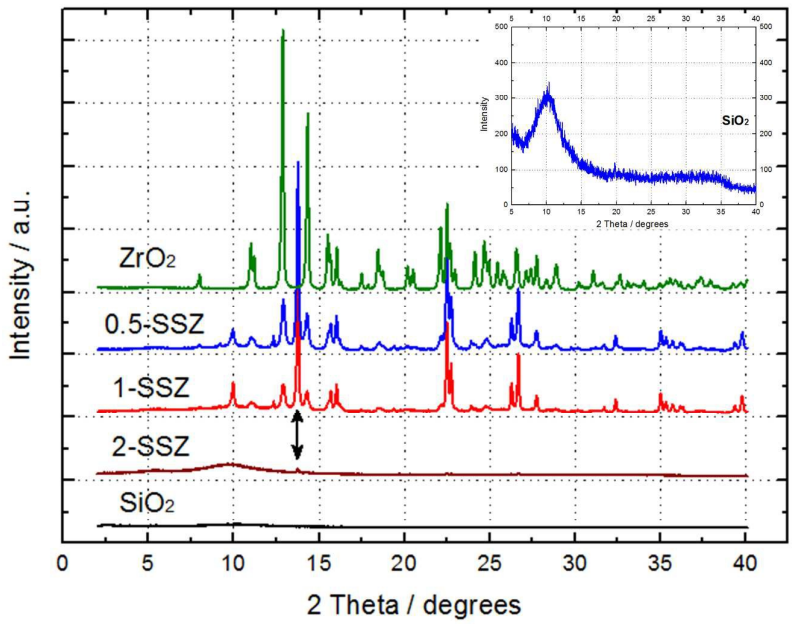

Figure 1. XRD patterns of the synthesized SSZs with Si/Zr molar ratios of 0.5, 1, and 2, pristine SiO_2, and ZrO_2, (inset) enlargement of XRD of SiO_2

The phases and structures of the synthesized SSZ powders were analyzed by X-ray diffraction (XRD, Mo-Kα1 radiation). Figure 1 shows the XRD patterns of the three synthesized SSZ powders with the different molar ratios at 1050 ^{o}C. To compare the patterns of the peaks from the SSZ powders, pristine SiO_2 and ZrO_2 powders were also measured. Sharp diffraction peaks were observed for 0.5 and 1-SSZ samples indicating the formation of a well crystalline structure. One broad peak at 2Θ=9.65 ^{o} and three small peaks at 13.7, 22.5, and 26.6 ^{o} were observed for 2-SSZ, indicating the reduced crystallinity of SSZ as compared with 2-SSZ. This could be nanocrystalline and/or amorphous structures. One broad band centered at around 9.65° in SiO_2 exhibited a sharper peak with a decrease in the Si/Zr molar ratio for the 1-SSZ. After that, the intensity of that peak was decreased for the 0.5-SSZ, and finally the peak was not observed for the ZrO_2. The change in this intensity can be explained as follows: the Si ions for the amorphous SiO_2 were replaced by Zr ions in the SSZ. The peak for 2Θ=13.7 was observed in all the SSZ samples; however, it was not detected in the SiO_2 and ZrO2 samples. This peak might be a unique peak for the crystal SSZ phase with the Si-O-Zr bonds.

View Article Online
DOI: 10.1039/C7DT01120B

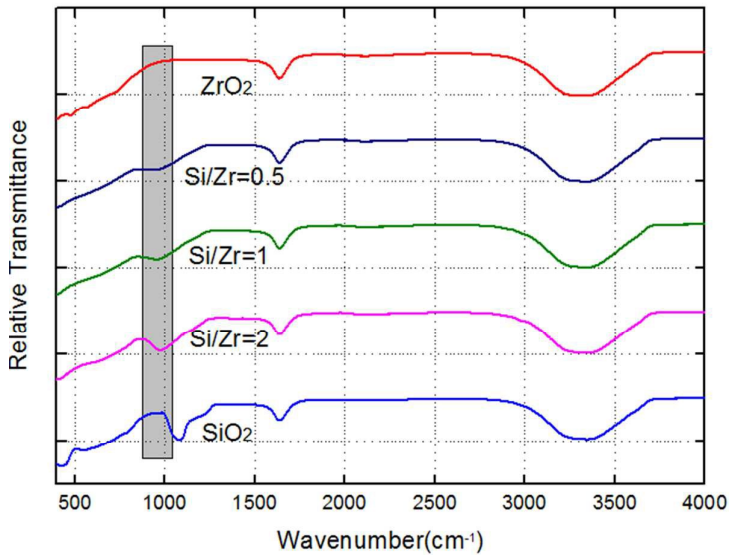

Figure 2. FT-IR of the synthesized SSZs with Si/Zr molar ratios of 0.5, 1, and 2, SiO_2, ZrO_2

The FT-IR spectra of the synthesized SSZ particles with the three different Si/Zr molar ratios (Si/Zr=0.5, 1, and 2), ZrO_2, and SiO_2 are shown in Figure 2. The spectra of these samples were taken in the spectral range of 4000 to 400 cm^{-1}. The band of ZrO_2 was shown at 480 cm^{-1}, and the bands of SiO_2 were observed at about 430, 780, 1080 and 1200 cm^{-1}. The ZrO_2 band at 480 cm^{-1} would be ascribed to the stretching frequency of Zr-O in pristine ZrO_2. SiO_2 bands at 430 and 780 cm^{-1} were associated with the Si-O-Si symmetric bond-bending vibration and bond-stretching vibration in pristine SiO_2, and the bands at 1080 and 1200 corresponded to the asymmetric bond stretching vibration of Si-O-Si. Each Si/Zr sample for the three molar ratios had Si-O-Zr bands centered at about 955 cm^{-1}. These results are within the reference range [22, 23]. By increasing the molar ratio of the Si/Zr, the band with the Si-O-Zr bond grew sharper in intensity. When compared to the band with the Si-O-Si bond (1080 cm^{-1}) for the pristine SiO_2, the stretching frequency of the Si-O-Zr band at 955 cm^{-1} is from the formation of a SSZ network as the replacement of the Si atoms proceeds [23]. The band at 1340 cm^{-1} is characteristic of the bridging OH group in $Zr(OH)_4$. The bands for the SSZs circa. 3300 cm^{-1} and circa. 1630 cm^{-1} are associated with the stretching and banding of water [24]. Therefore, these result showed that the particles of the three different SSZs were prepared successfully, indicated by the presence of Si-O-Zr bond in each sample.

View Article Online
DOI: 10.1039/C7DT01120B

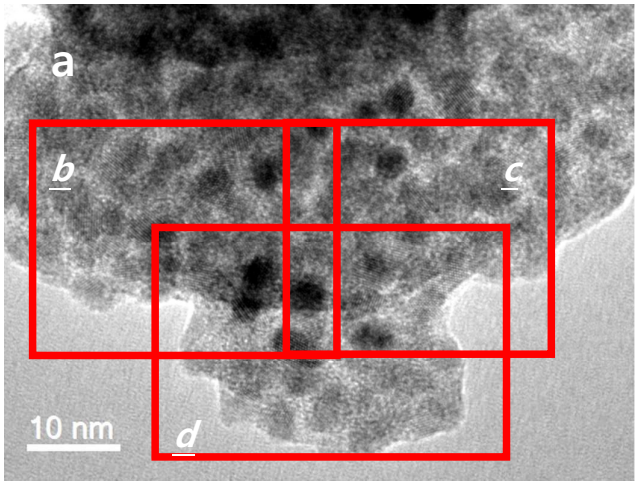

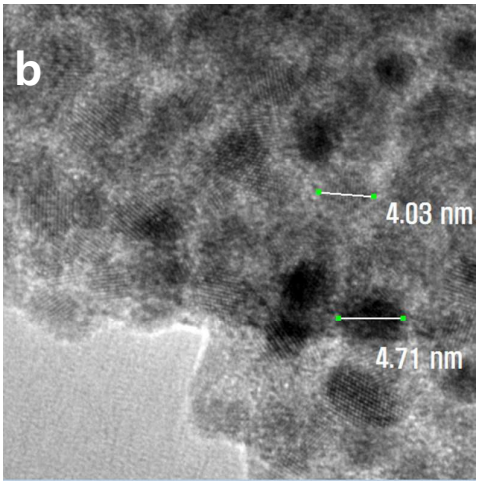

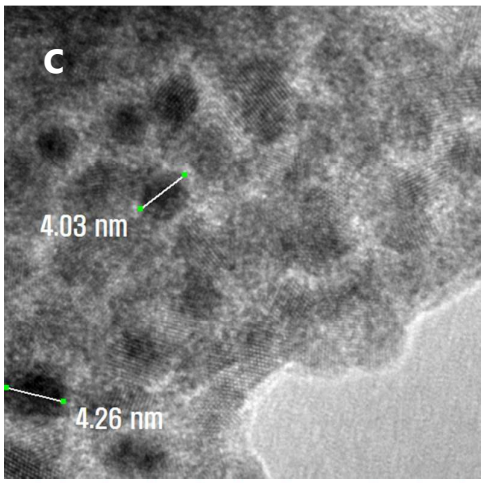

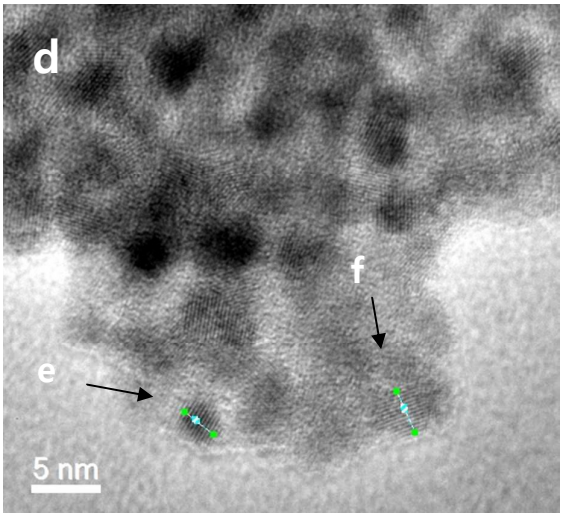

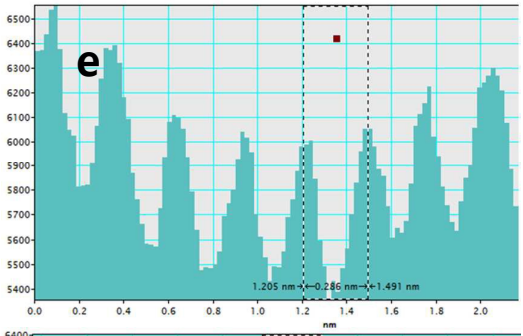

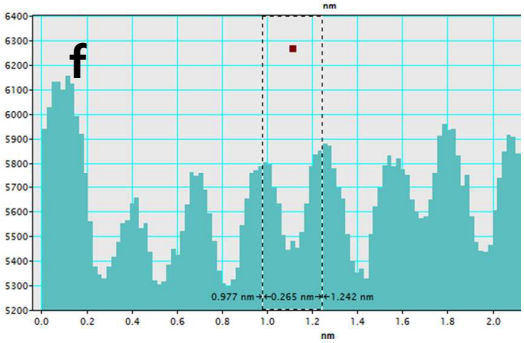

View Article Online
DOI: 10.1039/C7DT01120B

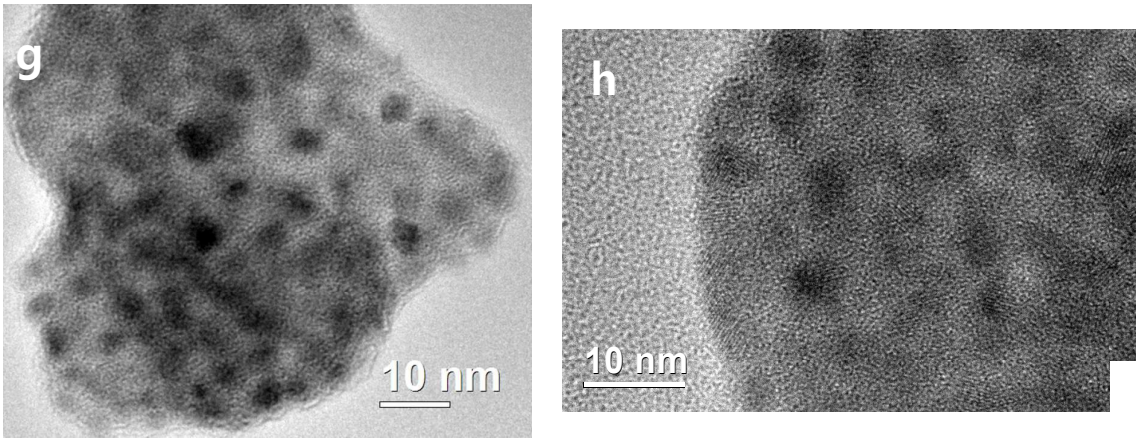

Figure 3.TEM images and the corresponding profiles of the 1- and 2-SSZ; (a) TEM image of 1-SSZ; (b, c, d) enlarged TEM image of (a); (e, f) Lattice fringes line profiles showing the lattice d-spacing from the area marked as 'e and f' in image 'd'; (g, h) TEM images of 2-SSZ with different magnifications

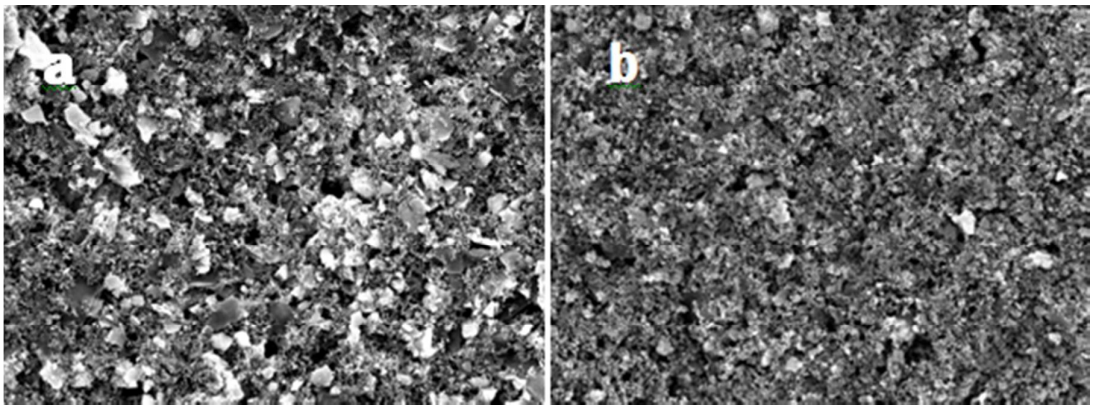

Figure 4.SEM micrographs of 1-SSZ (a) and 2-SSZ (b)

TEM and SEM were used to analyze the crystalline feature and morphology of the SSZs. Figure 3 shows the high-resolution TEM images of the 1-SSZ and 2-SSZ particles. The images of (a, b, c, d) were taken from the sample of 1-SSZ, and the (g, h) images were obtained from 2-SSZ. The size of nanoparticles had a diameter of circa. 4 - 5 nm in the images (b, c). The lattice fringes were clearly observed, and the lattice plane distance was calculated as 0.286 nm in Figure 3(e), which belongs to the tetragonal-ZrO_2 (0.29 nm) [25]. Another lattice plane distance was calculated as 0.265 nm (Figure 3(f)), this value matched with the interplanar distance of the plane (110) in the SiO_2 reference (0.26 nm) [26]. These TEM results confirmed the nanocrystal particles, which consisted of SiO_2 and ZrO_2. The

View Article Online
DOI: 10.1039/C7DT01120B

majority of 2-SSZ particles were amorphous as shown in the image (figure (g)), with very low crystallinity as indicated by the slight lattice fringe lines (figure (h)). Whereas, the TEM images (a, b, c, d) of 1-SSZ clearly showed that the dominant crystalline structure. These results were in agreement with the results obtained by XRD. Figure 4 shows the SEM images of the different structure for the 1-SSZ(left) and for the 2-SSZ(right) electrodes at the same magnification, respectively. Figure 4(a) showed much more crystalline image than figure 4(b). These different images support the results of the TEM and the XRD analyses.

Galvanostatic charge/discharge curves obtained in the voltage range of 0.001 and 2.0V (Li/Li^+) at a current density of 100 mA g^{-1} were obtained to investigate the electrical reactıvity of each electrode. Figure 5 (a, b, c) shows the charge/discharge profiles for the three samples (0.5-, 1-, 2-SSZ) at different cycles. Figure 5(d) shows the cycling performance of 0.5-, 1-, and 2-SSZ. There is obviously one plateau for each curve, which does not appear after the 1st cycle, and this discharge plateau in the voltage around 0.6-0.7 V is associated with the formation of a solid electrolyte interface (SEI) film and the decomposition of the electrolyte. The 1st and 2nd discharge capacities of 2-SSZ were 1237 and 543 mAh g^{-1}, respectively, and its capacity at the 30th cycle was 461 mAh g^{-1}(see figure 5(c)). As shown in figure 5 (b) and (a), the discharge capacities of the 1st and 2nd cycle of 1-SSZ were 964 and 323, and the capacities of 0.5-SSZ were 478 and 169 mAh g^{-1}, respectively. The figure 5 (c) shows that there is a difference between the charge capacity and the discharge capacity of 2-SSZ. This could be due to the different structures among 2-SSZ, 1-SSZ, and 0.5-SSZ, where 2-SSZ was mainly amorphous structure whereas 1-SSZ and 0.5-SSZ contained predominantly the crystalline structure.

Based on the capacity results of three electrodes, the 2-SSZ electrode has a better capacity and cyclability than that of the other two electrodes. Two possible reasons can explain these results. The first reason is the different mechanism for the insertion reaction between the guest and host materials. The second reason is the structural difference between the amorphous and crystalline structure.

View Article Online
DOI: 10.1039/C7DT01120B

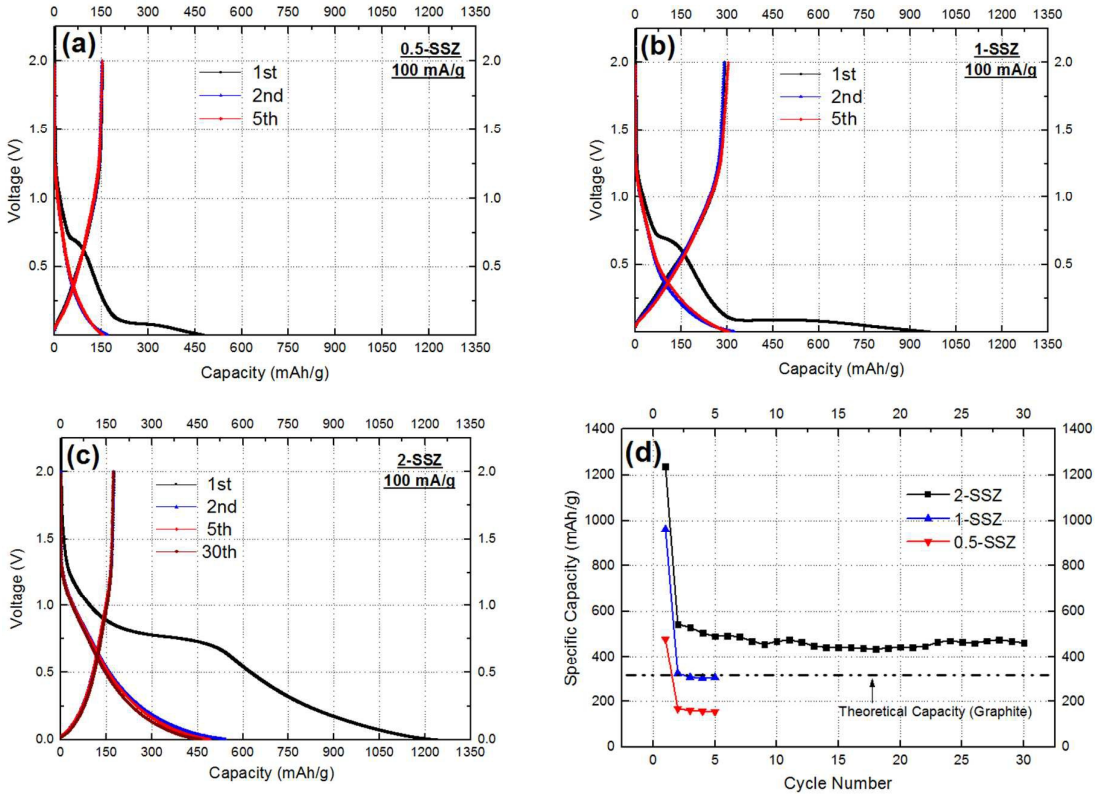

Figure 5. Galvanostatic discharge/charge voltage profiles of the SiO_2/ZrO_2 with the three different molar ratios ((a):0.5-, (b):1-, and (c): 2-SSZ), comparison of long-term cycle tests (d)

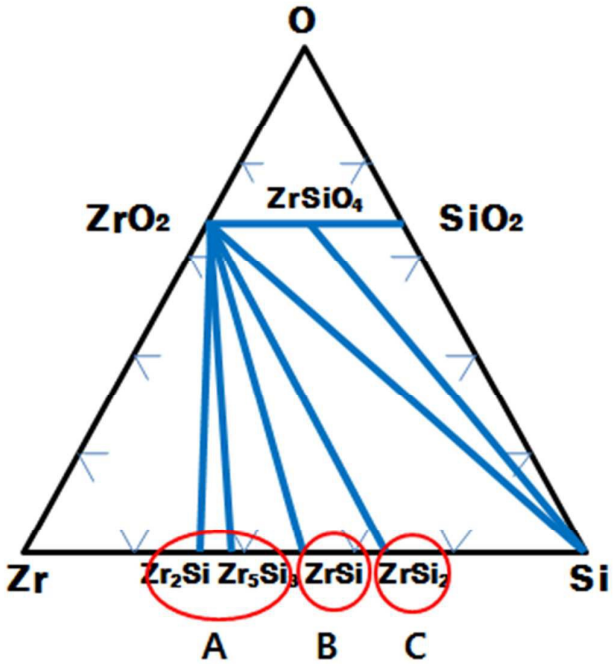

Figure 6. Ternary Phase Diagrams for Zr-O-Si [27]

View Article Online
DOI: 10.1039/C7DT01120B

Firstly, the reason why the capacity is different is related to the different mechanisms of the reactions between the lithium ions of the guest species and the possible materials (e.g. $ZrSi_2$, ZrSi, or Zr_2Si or Zr_5Si_3) formed by each of the host materials (2-, 1-, or 0.5-SSZ) during the repeated cycles. In order to understand the phases of the SSZs with three different molar ratios calcined at 1050 ^oC, a phase diagram was used [27]. Figure 6 is the ternary phase diagram of Zr-O-Si at 900 ^oC. Although all the phases of SSZs cannot be known from this figure because of the difference in the calcination temperatures (900 and 1050 ^oC), some information from this figure may be obtained to understand the phases of the SSZs with three different molar ratios. Typically, the final main reversible reaction of SiO_2 with lithium ions is the reactions of Si and Li-ions as shown below.

$$Si + xLi^+ + xe^- \leftrightarrow Li_xSi$$

Therefore, when the above reaction and phase diagram are considered together, in the case of the three SSZs, the final reversible reactions can be understood as the reactions of Zr_2Si and (or) Zr_5Si_3 from 0.5-SSZ, ZrSi from 1-SSZ, and $ZrSi_2$ from 2-SSZ, with Li-ions. This can be summarized as follows:

Circle	Chemical Reaction		Thermodynamics
A: 0.5-SSZ	$ZrSiO_4 + 8Li^+ + 8e^- \rightarrow 4Li_2O + (1/2)Zr_2Si + (1/2)Si$	(A1)	Reaction (A1; B1; C1; D1): $\Delta G^o<0$, $\Delta H^o<0$, $\Delta S^o<0$ • Spontaneous • Exothermic reaction • Decrease in entropy
	$(1/2)Zr_2Si + xLi^+ + xe^- \leftrightarrow (1/2)Li_xZr_2Si$	(A2)	
	$ZrSiO_4 + 8Li^+ + 8e^- \rightarrow 4Li_2O + (1/5)Zr_5Si_3 + (2/5)Si$	(B1)	
	$(1/5)\ Zr_5Si_3 + xLi^+ + xe^- \leftrightarrow (1/5)Li_xZr_5Si_3$	(B2)	
B: 1-SSZ	$ZrSiO_4 + 8Li^+ + 8e^- \rightarrow 4Li_2O + ZrSi$	(C1)	
	$ZrSi + xLi^+ + xe^- \leftrightarrow Li_xSiZr$	(C2)	
C: 2-SSZ	$2ZrSiO_4 + 12Li^+ + 12e^- \rightarrow 6Li_2O + ZrSi_2 + ZrO_2$	(D1)	
	$ZrSi_2 + xLi^+ + xe^- \leftrightarrow Li_xSi_2Zr$	(D2)	

Each initial chemical reaction is shown as a spontaneous and exothermic reaction with a decrease in entropy. These conditions indicate that only spontaneous reactions occur at the following temperatures ($T=\Delta H/\Delta S$): T= 1759 K in reaction (A1), 1184 K in reaction (B1), 607

View Article Online
DOI: 10.1039/C7DT01120B

K in reaction (C1), 5340 K in reaction (D1). Hense, it can be confirmed that the four reactions above occurred as spontaneous reactions, during the battery-test because the experiments were performed at room temperature of 298 K. The material density values of Zr_2Si, Zr_5Si_3, ZrSi, and $ZrSi_2$ are 5.972, 5.777, 5.554, and 4.84 gm/cc, respectively [28]. We observed that the density decreased as the molar ratio of Si was increased, indicating a larger possible reaction area for the guest species (lithium ions) at the empty interstitial site in the host materials. A smaller density and the Zr fraction provided an increased space to accommodate a volume expansion and enhanced the average lattice constant and the diffusion coefficient of the Li-ions. These improvements may affect the structural change by the lattice distortion into minimum. These finally caused an increase in the Li-ions diffusivity, and strongly supported the electrochemical characteristics with a large reactivity for the Li-ions. The benefit of $ZrSi_2$ led to a better reversible capacity with little pulverization as compared to that of the other compounds. These resulted in enhancing the capability of the reversible capacity and the superior cycling performance as compared to the others.

The second reason is the effect of different structure. Based on the results of XRD and TEM measurements, 0.5- and 1-SSZs have a typical crystalline structure. The structure of 2-SSZ has a majorly amorphous structure, which included with some crystalline structure. The literature states that the amorphous structure has better cycling performance as compared to the crystalline [29, 30]. The crystalline structure would provide efficient pathways for electron transport to enhance the electrical conductivity and support the mechanically stable structure to reduce the volume expansion [31]. Thus, the combination of these structures suppressed the volume change of 2-SSZ, and finally resulted in an increased reversible capacity.

Conclusions

This paper was preceded to unveil the mechanisms through electrochemical analysis and to understand the effect of different Si/Zr molar ratios on novel anode material SSZ. The SSZ electrodes delivered a superior capacity when the molar ratio of Si/Zr was increased from 0.5 to 2. The specific capacity of 2-SSZ was much higher than that of 0.5- or 1-SSZ. The 2-SSZ electrode also had superior cycling performance. This could be due to the formation of $ZrSi_2$ by 2-SSZ which would provide more effective reactivity with Li-ions intercalation and deintercalation upon Li-ions diffusion than that of Zr_2Si or Zr_5Si_3 from

View Article Online
DOI: 10.1039/C7DT01120B

0.5-SSZ or ZrSi from 1-SSZ. This result indicated that $ZrSi_2$ increased the possible reaction area for the guest species (lithium ions) at the empty interstitial site in the host materials. It could provide a large space to accommodate volume expansions, and it was supportive by maintaining the lattice constant and reducing the ratio of the structural distortion. In addition, 2-SSZ structure consisted of a majorly amorphous structure with a crystalline structure related to the Zr-O-Si bond. Such combined structutre was advantageous in providing a good capacity through amorphous structure and such efficient pathway for electron transport and little pulverization through the crystalline structure. With such benefits, the drastic volume expansion was reduced during repeated cycles, which led to the enhanced reversible capacity and the cyclability. This paper provides a fundamental understanding on the rational design of efficient binary oxide materials for lithium ions batteries and serves as a guide to help to determine the optimal performance of binary oxides.

View Article Online
DOI: 10.1039/C7DT01120B

References

1. Bruce, P.G., B. Scrosati, and J.-M. Tarascon, *Nanomaterials for Rechargeable Lithium Batteries.* Angewandte Chemie International Edition, 2008. **47**(16): p. 2930-2946.
2. Dunn, B., H. Kamath, and J.-M. Tarascon, *Electrical Energy Storage for the Grid: A Battery of Choices.* Science, 2011. **334**(6058): p. 928-935.
3. Yi, T.-F., et al., *Spinel Li4Ti5−xZrxO12 (0 ⩽ x ⩽ 0.25) materials as high-performance anode materials for lithium-ion batteries.* Journal of Alloys and Compounds, 2013. **558**(0): p. 11-17.
4. Nan, D., et al., *Highly porous carbon nanofibers from electrospun polyimide/SiO2 hybrids as an improved anode for lithium-ion batteries.* Electrochemistry Communications, 2013. **34**(0): p. 52-55.
5. Kil, E.-H., et al., *Imprintable, Bendable, and Shape-Conformable Polymer Electrolytes for Versatile-Shaped Lithium-Ion Batteries.* Advanced Materials, 2013. **25**(10): p. 1395-1400.
6. Company, N. *About Li-ion batteries.* [cited 2015 Feb. 10th]; Available from: www.nexeon.co.uk.
7. Wu, H.B., et al., *Nanostructured metal oxide-based materials as advanced anodes for lithium-ion batteries.* Nanoscale, 2012. **4**(8): p. 2526-2542.
8. Deng, D., et al., *Green energy storage materials: Nanostructured TiO2 and Sn-based anodes for lithium-ion batteries.* Energy & Environmental Science, 2009. **2**(8): p. 818-837.
9. Liu, X., et al., *Sandwich Nanoarchitecture of Si/Reduced Graphene Oxide Bilayer Nanomembranes for Li-Ion Batteries with Long Cycle Life.* ACS Nano, 2015. **9**(2): p. 1198-1205.
10. Wen, Z., et al., *Silicon nanotube anode for lithium-ion batteries.* Electrochemistry Communications, 2013. **29**: p. 67-70.
11. Zhao, Y., et al., *Hierarchical micro/nano porous silicon Li-ion battery anodes.* Chemical Communications, 2012. **48**(42): p. 5079-5081.
12. Schmidt, V., et al., *Silicon Nanowires: A Review on Aspects of their Growth and their Electrical Properties.* Advanced Materials, 2009. **21**(25-26): p. 2681-2702.
13. Chan, C.K., et al., *High-performance lithium battery anodes using silicon nanowires.* Nat Nano, 2008. **3**(1): p. 31-35.
14. Yao, Y., et al., *Carbon-coated SiO(2) nanoparticles as anode material for lithium ion batteries.* Journal of Power Sources, 2011. **196**(23): p. 10240-10243.
15. Gao, B., et al., *Alloy formation in nanostructured silicon.* Advanced Materials, 2001. **13**(11): p. 816-+.
16. Yu, Y., et al., *Electrochemical performance of nano-SiO2 modified LiCoO2 thin films fabricated by electrostatic spray deposition (ESD).* Electrochimica Acta, 2006. **51**(16): p. 3292-3296.
17. Liu, J., et al., *Ultrathin atomic layer deposited ZrO2 coating to enhance the electrochemical*

View Article Online
DOI: 10.1039/C7DT01120B

performance of Li4Ti5O12 as an anode material. Electrochimica Acta, 2013. **93**(0): p. 195-201.

18. Cho, J., et al., *Zero-strain intercalation cathode for rechargeable Li-ion cell.* Angewandte Chemie-International Edition, 2001. **40**(18): p. 3367-+.
19. Chen, Z.H. and J.R. Dahn, *Effect of a ZrO2 coating on the structure and electrochemistry of LixCoO2 when cycled to 4.5 V.* Electrochemical and Solid State Letters, 2002. **5**(10): p. A213-A216.
20. Chung, K.Y., et al., *In situ XRD studies of the structural changes of ZrO2-coated LiCoO2 during cycling and their effects on capacity retention in lithium batteries.* Journal of Power Sources, 2006. **163**(1): p. 185-190.
21. Tarafdar, A., A.B. Panda, and P. Pramanik, *Synthesis of ZrO2–SiO2 mesocomposite with high ZrO2 content via a novel sol–gel method.* Microporous and Mesoporous Materials, 2005. **84**(1–3): p. 223-228.
22. Castro, Y., et al., *Silica-zirconia sol-gel coatings obtained by different synthesis routes.* Journal of Sol-Gel Science and Technology, 2005. **35**(1): p. 41-50.
23. Lee, S.W. and R.A. Condrate, *The Infrared and Raman-Spectra of Zro2-Sio2 Glasses Prepared by a Sol-Gel Process*. Journal of Materials Science, 1988. **23**(8): p. 2951-2959.
24. Lopez, T., et al., *Preparation of Sol-Gel Sulfated Zro2-Sio2 and Characterization of Its Surface-Acidity.* Applied Catalysis a-General, 1995. **125**(2): p. 217-232.
25. Polli, A.D., et al., *Structural characterization of ZrO2 thin films produced via self-assembled monolayer-mediated deposition from aqueous dispersions.* Thin Solid Films, 2000. **379**(1–2): p. 122-127.
26. Jiao, J., Q. Xu, and L. Li, *Porous TiO2/SiO2 composite prepared using PEG as template direction reagent with assistance of supercritical CO2.* Journal of Colloid and Interface Science, 2007. **316**(2): p. 596-603.
27. Sinclair, R., *Properties of Metal Silicides*. Vol. 14. 1995: Institution of Engineering and Technology.
28. *materials project*. 2016; Available from: https://materialsproject.org/#search/materials/{"nelements"%3A2%2C"elements"%3A"Zr-Si"}.
29. Maranchi, J.P., A.F. Hepp, and P.N. Kumta, *High Capacity, Reversible Silicon Thin-Film Anodes for Lithium-Ion Batteries.* Electrochemical and Solid-State Letters, 2003. **6**(9): p. A198-A201.
30. Yin, J., et al., *Micrometer-Scale Amorphous Si Thin-Film Electrodes Fabricated by Electron-Beam Deposition for Li-Ion Batteries.* Journal of The Electrochemical Society, 2006. **153**(3): p. A472-A477.
31. Cui, L.-F., et al., *Crystalline-Amorphous Core−Shell Silicon Nanowires for High Capacity and High Current Battery Electrodes.* Nano Letters, 2009. **9**(1): p. 491-495.